Tellus (1982), *34*, 555–566

A numerical simulation of an atmospheric vortex street

By PAUL H. RUSCHER and J. W. DEARDORFF, *Department of Atmospheric Sciences, Oregon State University, Corvallis, Oregon 97331, USA*

(Manuscript received December 1, 1981; in final form February 23, 1982)

ABSTRACT

A mesoscale mixed-layer model of the planetary boundary layer is applied to the flow past a mountain island during a cold air outbreak over the Kuroshio Current. Utilizing data taken during AMTEX '75, the governing equations are integrated in time to simulate development of a Kármán vortex street downstream of the island of Cheju-do. The use of open lateral boundary conditions and an encroachment scheme which allows some mountain grid points to experience occasional encroachment of mixed-layer fluid as the mixed-layer deepens (and decroachment as the mixed layer thins) is also discussed.

Comparing various non-dimensional parameters on vortex-street characteristics, it is shown that the simulated vortex street resembles the observed atmospheric one rather well. Uncertainty in formulating the proper value of the eddy viscosity and the implication this has on Reynolds number comparisons are also discussed.

1. Introduction

The planetary boundary layer (PBL) is the lowest region of the atmosphere in which vertical transfer of momentum, heat, and moisture occurs continuously and on rather small scales. This makes modeling the motion in the PBL a very complicated procedure. However, on certain occasions the PBL may be well-mixed so that detailed vertical resolution in the numerical model is no longer required. Such a mixed-layer model, which only dates back to the pioneering work of Lilly (1968) and Lavoie (1972) barely a decade ago, has been used to simulate many meteorological phenomena whose spatial and temporal variability is in the mesoscale range.

Initially the mesoscale mixed-layer model (MMM) was used to model steady state features. Lavoie (1972) used the model to simulate lake-effect snowstorms over western New York State and Pennsylvania. He later (Lavoie, 1974) used the model to simulate the flow in the vicinity of the island of Oahu, Hawaii and accurately simulated not only the general flow features but also the rainshadow effect. Other researchers also used the model in the late 60s and early 70s to study the importance of horizontal asymmetries on the tropical mixed layer, the effect of the urban heat island on the mixed layer, and air pollution.

Because the MMM appeared so promising over its first decade of use, it was ultimately used in a predictive mode. Keyser and Anthes (1977) used the model to predict the flow over the middle Atlantic states and were able to simulate the lower part of the sea breeze circulation. Price et al. (1978) used a mixed-layer model to simulate storm-induced oceanic mixed-layer deepening in the Gulf of Mexico. Overland et al. (1979) used the MMM to study the channeling effect of flow through the Straight of Juan de Fuca bordering the State of Washington and Province of British Columbia.

These attempts all met with moderate success. However, in a comparison of a three-dimensional mesoscale model and the model of Keyser and Anthes (1977), Anthes et al. (1980) concluded that the MMM was not capable of forecasting the sea breeze over variable topography well. A part of the discrepancy in the results of the two models may be due to exclusion of advection of horizontal momentum just above the top of the mixed layer in the MMM. Further experiments have been performed and are discussed by Anthes et al. (1982).

0040-2826/82/060555-12$02.50/0

The purpose of this paper is to utilize a simplified MMM to study the flow past an ocean island during a case of cold air outbreak over the Kuroshio Current. The flow feature of interest is the atmospheric analog to the Kármán vortex street, which was visible in the stratocumulus clouds in the well-mixed PBL downstream of the island of Cheju-do, Republic of Korea, on February 17, 1975. To our knowledge, the vortex street has not previously been numerically predicted in the atmospheric PBL using a numerical model.

2. The model

2.1. *The physical model*

This section will detail the idealized atmospheric structure of the model and the governing equations. Fig. 1 is an idealized look at the vertical profiles of potential temperature, wind velocity, and specific humidity in the lowest few kilometers of the atmosphere. There are four layers in the sketch (from bottom to top): the unstable surface layer, the well mixed layer (of depth h above sea level), the inversion layer of assumed constant strength $\Delta\theta$, where θ is potential temperature, and the overlying stable atmosphere. Although the theoretical model involves these four distinct regions of the atmosphere, we are concerned with the development of only the mixed layer. Therefore the other three regions will receive only brief attention.

The surface layer, typically considered to be about 50 m deep, supplies heat to the mixed layer and extracts momentum from it. The overlying inversion, extending from $h^- < z < h^+$ (see Fig. 1), acts as a lid on convection in the mixed layer. The strength of the inversion is important in determining the magnitude of the pressure gradient force in the mixed layer where its top slopes. The stable atmosphere just above $z = h$ is assumed to be barotropic so that the synoptic-scale pressure gradient which forces the mixed-layer flow from above is constant; thus we do not treat the overlying stable atmosphere.

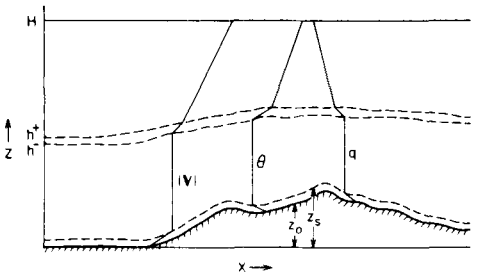

Fig. 1. Vertical profiles of potential temperature (θ), velocity ($\mathbb{V}$), and specific humidity (q) in the well-mixed PBL.

We will be applying the MMM to a geophysical fluid flow problem which is governed primarily by diffusion and advection of vorticity near an obstacle. We have therefore deemed it unnecessary in this simplified study to include in the model temporal and spatial variability of potential temperature in the PBL, surface heat flux, mixed-layer entrainment, or moisture budget. These physical processes are normally included in MMM's; however, their exclusion here is assumed not to affect strongly the solution to the problem of vortex development.

The basic equations governing the mean flow ($\mathbb{V}$) in the mixed layer are the primitive equations. Using a cartesian coordinate system applied on an f-plane, the equations are vertically averaged through the mixed layer to reduce the problem to a two-dimensional one in the horizontal. We finally obtain, after Reynolds averaging

$$\frac{\partial \mathbb{V}}{\partial t} = -\mathbb{V}\cdot\nabla\mathbb{V} - f\hat{k}\times(\mathbb{V}-\mathbb{V}_g) - g\frac{\Delta\theta}{\theta}\nabla h - \frac{c_D|\mathbb{V}|\mathbb{V}}{h-z_s} + \nabla\cdot(K_v\nabla\mathbb{V}) \tag{1}$$

and

$$\frac{\partial h}{\partial t} = -\nabla\cdot(h-z_s)\mathbb{V} + \nabla\cdot(K_h\nabla h), \tag{2}$$

where f is the coriolis parameter, $\hat{k}$ is the vertical unit vector, $\mathbb{V}_g$ is the constant geostrophic wind imposed just above $z = h$, g is the acceleration of gravity, c_D is the coefficient of surface drag, z_s is the height of the surface layer above sea level, K_v is the coefficient of eddy diffusivity for momentum, and K_h is the coefficient of eddy diffusivity for h.

Although there are inconsistencies involved in assuming that $\mathbb{V}_g$ and $\Delta\theta$ are constant in space and time while h is variable (Anthes et al., 1982), it is not yet clear that inclusion of a prognostic buffer layer between h^- and some greater undisturbed height would materially improve the model.

The last term of each of the above equations,

representing horizontal diffusion of momentum and mass, respectively, by subgrid-scale processes, may be expressed in terms of an eddy diffusivity using, for example, either the form of Smagorinsky (1963):

$$K_v = \frac{C^2 (\Delta s)^2}{\sqrt{2}} \left\{ \left(\frac{\delta u_i}{\delta x_j} + \frac{\delta u_j}{\partial x_i} \right)^2 \right\}^{1/2}, \quad i,j = 1, 2; \quad (3)$$

or of Leith (1969):

$$K_v = \gamma_2 |\nabla \zeta| (\Delta s)^3, \quad (4)$$

where C and γ_2 are dimensionless constants and Δs is the grid spacing on a square grid. K_h is taken to be $\frac{1}{2}$ the value of K_v in the same grid box.

An interesting aspect of our application of this model is that the peak of Cheju-do is higher than the observed mixed-layer depth during the three days the vortex street was observed. Fig. 2 shows the topography of Cheju-do; notice not only the rather high peak (1950 m) but also the symmetric elliptical shape of the island. The next subsection describes the numerical aspects.

2.2. *The numerical model*

After breaking (1) into component equations and using the vector-invariant form (Arakawa and Lamb, 1977), an energy-conserving finite difference scheme of Sadourny (1975) is applied on a horizontally staggered "C" grid (Mesinger and Arakawa, 1976). This particular choice of grid is most advantageous for atmospheric models because of its generally superior dispersion characteristics. The equations are explicitly integrated through time using the leapfrog method. To suppress decoupling of the physical and computational modes (Haltiner, 1971), a time-averaging operator suggested by Keyser and Anthes (1977) is applied every 18 time steps.

The time step in the model is limited by the phase speed of the fastest-moving wave in the system and through the Courant–Friedrichs–Lewy (CFL) stability criterion. The fastest-moving wave is an external or interfacial gravity wave (Lavoie, 1972) at the inversion level, with a phase speed as high as 35 m s^{-1}. For the grid size used in this experiment ($\Delta x = \Delta y = 7$ km or 5 km), the time step used can be about 100 s or 75 s, respectively. Another numerical stability requirement is on the frictional terms, but because the eddy diffusivities generated by (3) and (4) are relatively small, the condition is easily met.

Cloud photographs from the Defense Military Satellite Program (DMSP) were analyzed for well-defined cases of the atmospheric vortex street. The most striking case occurred on February 17, 1975, a time during which the Air Mass Transformation Experiment (AMTEX) was being conducted. The aerological data given by Agee and Lomax (1978) and in the data volume published by the Management Committee for the AMTEX, 1975 (AMTEX 75 Data Report, Volume 2) were used to supply the average geostrophic wind in the mixed layer (9·7 m s^{-1}) and an initial mean height (890 m) of the inversion. The value assigned to $\Delta\theta/\theta$ was

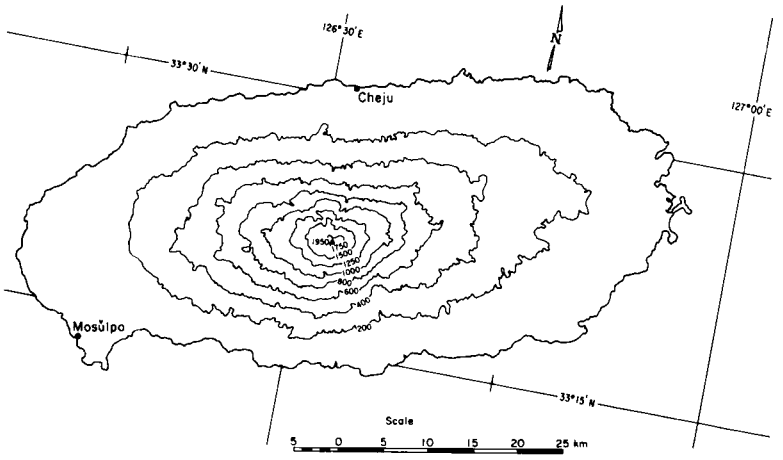

Fig. 2. Topographic map of Cheju-do, Republic of Korea.

0.034, and drag coefficients of $c_D = 7.0 \times 10^{-3}$ and $c_D = 1.5 \times 10^{-3}$ were used over land and water, respectively.

For the initial mixed-layer velocities in the experiments, values are used resulting from the solution of the steady-state, vertically-integrated Ekman balance:

$$f\hat{k} \times (\mathbb{V} - \mathbb{V}_g) = \frac{c_D |\mathbb{V}| \mathbb{V}}{h - z_s}. \tag{5}$$

These initial velocities were then smoothed using a nine-point smoothing operator (Haltiner, 1971). The topography used in the experiment is a subjectively-smoothed representation of Cheju-do (whose topography is shown in Fig. 2) which preserves symmetry in the direction perpendicular to the flow. Where the mountain was higher than the mixed-layer top minus 10 m, $h - z_s$ was set equal to ten meters and the normal velocity components of the appropriate grid box were set equal to zero.

The problem of lateral boundary conditions in a model of this type is not simple because no well-posed boundary conditions exist for such a system (Sundström and Elvius, 1979). Potential problems which need to be addressed are the overspecification of boundary values (Chen, 1973) and false reflection of waves at an outflow boundary (Nitta, 1964; Matsuno, 1966). The boundary condition chosen here is a modified version of the radiation condition posed by Orlanski (1976). Local phase speeds for each prognostic variable are computed at each boundary point. If the boundary is an outflow point, the modified radiation condition is imposed. If the point is inflow, we assume the flow is in a vertically-integrated Ekman balance, so that the solution of (5) is once again utilized. The outflow modification, suggested by Klemp and Wilhelmson (1978), is illustrated in the following equation valid for the zonal component of velocity at a zonal outflow boundary point:

$$\frac{\partial u}{\partial t} + c_u \frac{\partial u}{\partial x} = f(v - v_g) - c_D \frac{|\mathbb{V}| u}{h - z_s} - v \frac{\partial u}{\partial y}, \tag{6}$$

where c_u is the local phase speed, and u and v are the zonal and meridional components of the mean mixed-layer wind velocity, respectively. In Orlanski's boundary condition, the right hand side of (6) is set to zero. However, as h and V gradually vary in time, these terms may not balance exactly and their omission at the boundaries could lead to spurious strong localized velocity gradients at the boundaries.

To suppress noise generated at inflow boundaries by overspecification of variables in Orlanski's boundary condition (Klemp and Lilly, 1978), we use a local smoother $(\frac{1}{4}, \frac{1}{2}, \frac{1}{4})$ which alters the value of the interior point closest to the inflow point. Chen (1973) has shown that this smoother effectively acts to suppress noise due to overspecification.

One feature of the numerical model needs to be explained in more detail. The mixed layer top is free to move up and down during model integration, so that at some point in time it might be suspected that more (or less) mountain grid points would be above the top of the mixed layer than were initially. If the mixed layer top is forecast by the model to be lower than the topography plus 10 m at a particular grid point, the normal velocity components are set equal to zero and the mixed-layer thickness set equal to ten meters. If, however, horizontal diffusion causes mixed-layer fluid to encroach on such an exposed grid point on the mountain, new values of the velocity components are reset (from zero) to an average of the surrounding mixed-layer velocities.

This feature of the model allows realistic treatment of the rise and fall of the mixed layer in a region of high topography, and may be important upon further development of the mixed-layer model in which investigators may not only be interested in mixed-layer winds but also the topography of the inversion surface in complex terrain.

3. Meteorological situation

At the start of the AMTEX '75 experiment, a cold air outbreak occurred over the East China Sea as a mass of cold air moved off the Asian mainland over the warm waters of the Kuroshio Current. On three consecutive days (February 15 through February 17), an atmospheric vortex street was observed in the daytime DMSP imagery (Jensen and Agee, 1978). Fig. 3 is a DMSP photograph of the vortex street at 0236 GMT (1136 Japan Standard Time) on February 17, 1975. Cheju-do is obscured by clouds in this photograph. Orientation with respect to the AMTEX network is illustrated in Fig. 1 of Agee and Lomax (1978).

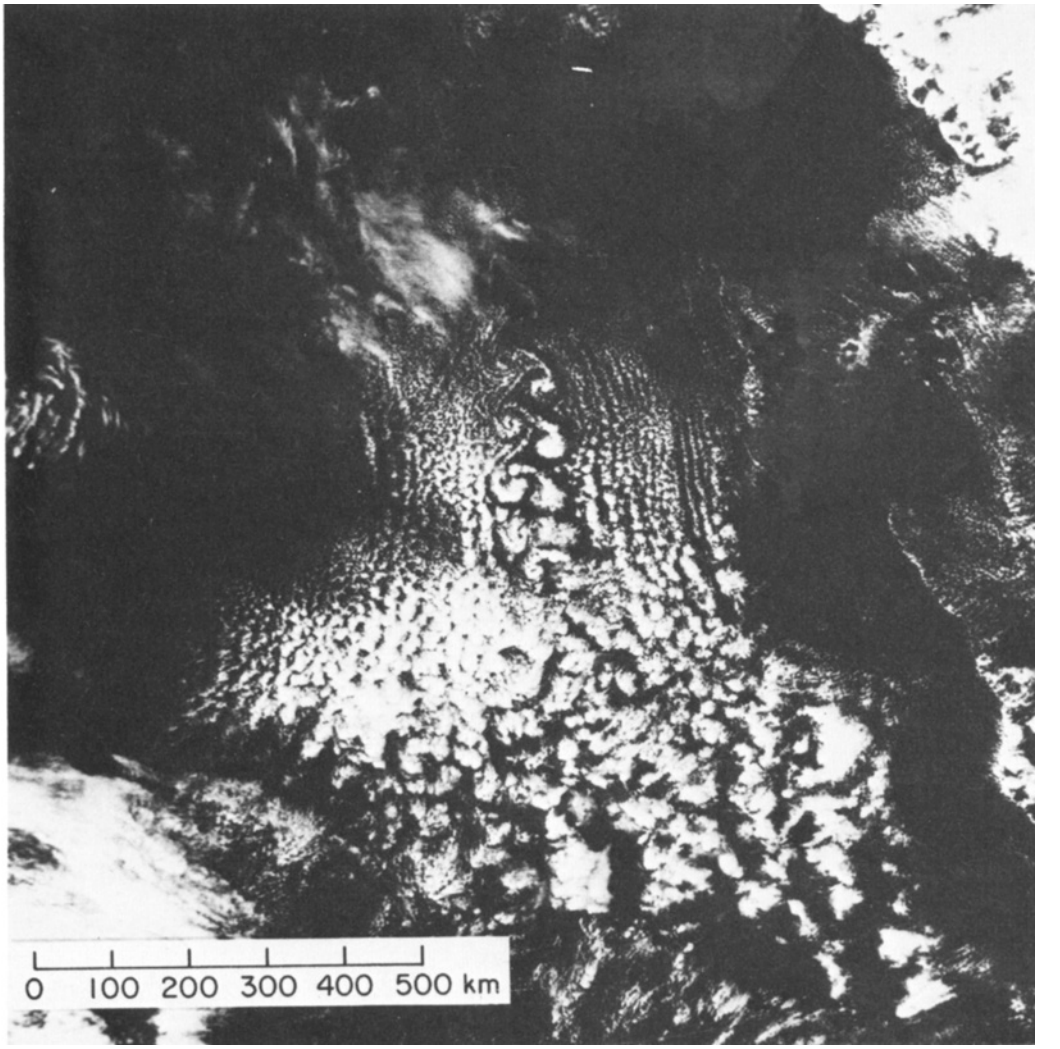

Fig. 3. Defense Military Satellite Program (DMSP) imagery over the AMTEX region at 0236 GMT on February 17, 1975.

The prevailing synoptic situation was a high pressure region over eastern China which set up a low-level northerly flow perpendicular to the largest diameter of Cheju-do (the major axis of the ellipse). The very cold air in contact with warm water (with air–sea temperature contrasts of about 10 °C) was an ideal situation for mesoscale cellular convection to develop (Agee and Lomax, 1978). The resultant upward heat flux allowed a convectively-mixed layer to form (in this case shallower than the peak of Cheju-do). Hence, Cheju-do effectively acted as a complete barrier to the flow in the PBL, forcing the air to flow around the island.

4. The vortex street

Tsuchiya (1969) observed a vortex street to the lee of Cheju-do under similar atmospheric conditions. Other researchers (e.g. Chopra and Hybert, 1964; Lyons and Fujita, 1968; Zimmerman, 1969; and Thomson et al. (1977)) have noted vortex

street formation in other areas of oceanic islands with high topography. The analogy between the Kármán and atmospheric vortex streets was first made by Chopra and Hubert (1964) and much of their work has been substantiated since that time. A comparison of the vortex street in Fig. 3 with laboratory photographs of a Kármán vortex street (e.g., Batchelor (1967); plate 2) does not reveal any major discrepancy. The mechanisms of formation of vortex streets in the flow past bluff obstacles is discussed in depth by Lamb (1932) and Abernathy and Kronauer (1962).

There are several non-dimensional parameters of importance in studying the vortex street, including the Reynolds number, $\mathrm{Re} = du_o/\nu$, where d is the cross-stream width of the obstacle to the flow, u_o is the flow speed outside the wake region, and ν is the molecular viscosity; Strouhal number, $\mathrm{S} = nd/u_o$, where n is the frequency of shedding of vortices; Lin's parameter $\beta = \mathrm{S}/\mathrm{Re}$; the spacing ratio, and the speed ratio. The spacing ratio is the ratio of the distance b between vortices taken perpendicular to the flow to the distance taken parallel to the flow, a. The speed ratio is the ratio of the vortex translation speed, u_e, to u_o. Each of these parameters has certain restricted ranges which have been observed to apply in both atmospheric and Kármán vortices.

Many studies have given evidence that the vortices observed to the lee of island peaks are Kármán analogies by noting similarities among the non-dimensional numbers (e.g. Chopra and Hubert, 1965; Zimmerman, 1969; Jensen and Agee, 1978). One thing noted in all these studies was the apparent discrepancy in the Reynolds number observed under the different cases. The range of the Reynolds number observed for regular Kármán vortices is from about 50 to 5000, while the atmospheric Reynolds number is of the order of 10^{10}. The approach utilized in resolving the discrepancy is to use an appropriate value of eddy viscosity ν_e to define an effective Re which then will fall within the proper range.

Many of the detailed studies on vortex streets have used circular cylinders or rectangular barriers as the obstacle to the flow. These include not only theoretical (e.g. Kármán, 1911; Gerrard, 1966) and laboratory studies (e.g. Kovásznay, 1949; Gaster, 1971), but also numerical simulations (e.g. Fromm and Harlow, 1963; Hirota and Miyakoda, 1965). In actuality, of course, mountain peaks more closely steep cones. Gaster (1969) studied vortex shedding from cones for neutral stratification and found multiple shedding frequencies at various heights. Trischka (1980) studied flow past six volcanic peaks by varying the shapes of smooth aluminium cones in a wind tunnel, attributing differences between observed atmospheric cases and simulated results to stratification in the atmosphere. Pao and Kao (1976), using spheres in a water tank, also discussed the effects of stability on the vortex street.

A numerical model of an atmospheric vortex street using a mixed-layer model would seem to be a logical progression in this sequence of studies on vortex streets. A further step would use a three-dimensional model and a conical obstacle. The next section will describe the types of experiments performed with our mixed-layer model and the results.

5. Numerical experiments

5.1. *Deep mixed layers*

Although the observations suggested the mixed layer to be shallower than the mountain peak (Jensen and Agee, 1978), we investigated the effect which mixed layers deeper than the peak would have on vortex street formation. This experiment had $\Delta x = \Delta y = 7$ km, and an initial depth of 3 km. After almost two hours, the flow had evolved to barely suggest a sinusoidal wake of very small amplitude, but no vortex street was present. Because other experiments with shallower mixed layers showed vortices downstream by this time, no further discussion of these results will be undertaken.

Experiments were also performed using an initial depth of two kilometers. The results (also not shown) are inconclusive. The encroachment scheme allowed one grid point to stick up above the inversion, so that the mountain was effectively a barrier, albeit a small one. The wind fields showed the presence of a wake-like disturbance of the island; however, no vortices persisted away from the island. The average diameter (20 km) of the obstacle in the mixed layer was not very large in comparison with the grid interval (7 km). The absence of vortices may have been due to this reason, or to the incomplete blockage of the flow in the vertical. A more realistic depth is used in the next experiment, which is discussed in the next subsection.

5.2. *Shallow mixed layer*

In this experiment, the MMM was run with the same grid spacing as in Exp. A, but the initial mixed-layer depth was specified to be 890 m, as mentioned earlier. We depict in Fig. 4 the flow after almost six hours. Cyclonic eddies are apparent downstream, but the field appears to be very noisy. Nevertheless, the familiar sinusoidal pattern is pronounced and the pattern suggested is similar to the general pattern of vortex streets. At this stage of the experimentation, we controlled the amount of noise in the field by varying the constant C in (3), although the strength of the vortices was also affected by the magnitude of the diffusion. We settled on a value for C of 0.15 for future use.

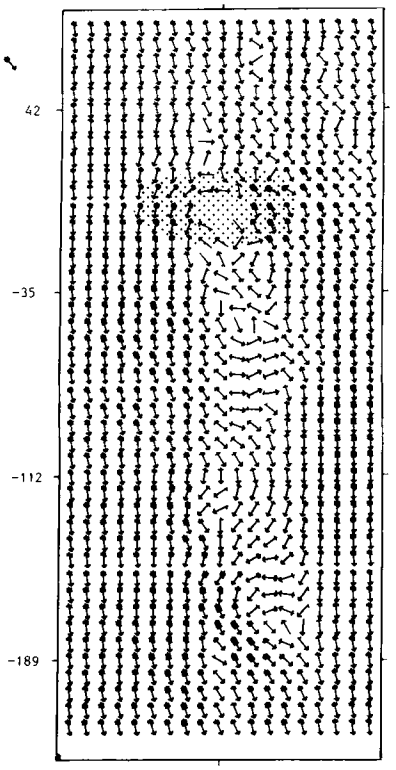

Fig. 4. Wind field and computational domain for Exp. B, $t = 5.83$ h. Stippled region indicates island position. Each half-barb is equal to 2.5 m s^{-1}. Scale along the y-axis is in km. The grid increment $\Delta s = 7$ km. The geostrophic wind vector is depicted in the upper-left corner of the figure.

5.3. *Higher resolution*

Our next runs were performed using the same mean mixed-layer depth but with a grid of higher resolution. The area of each grid box was cut almost in half by reducing the grid increment to 5 km. Fig. 5a shows the initial conditions for the higher-resolution grid. Points in the center of the mountain lie above the mixed layer and hence no vectors are plotted there. The flow for this experiment after almost six hours of integration time had elapsed is shown in Fig. 5b. By examining the vector plots after four and five hours of elapsed time, we were able to identify the three cells in Fig. 5b as the second cyclonic cell (2C, at $y = -93$ km), the second anticyclonic cell (2A, at $y = -50$ km), and the third cyclonic cell (3C, at $y = -23$ km). That we can no longer discern cells 1A and 1C may not be unrealistic—we would expect the cells to weaken downstream. This particular feature does not match the actual case in appearance, however, where several cells were observed beyond 100 km (see Fig. 3).

The flow field for this experiment is much improved over Exp. B, however. By reducing the grid spacing, the amount of noise (for the same size of the constant C) has been substantially reduced. Also, three cells are present in Fig. 5b, while there are only two present in Fig. 4. The boundary condition appears to be handling the situation well at the south, west, and east boundaries. However, the flow in the northern part of the domain appears to have been affected by some computational reflection. Miyakoda and Rosati (1977) also found some reflection to Orlanski's boundary condition.

Fig. 5c depicts the flow after almost nine hours of integration time. The vortices are being advected downstream and are diffusing rapidly. The vortices which appear here are vortices 3C ($y = -150$ km) and 4A ($y = -23$ km). Before discussing the comparison between this experiment and observed cases, however, we will briefly mention one further experiment performed.

5.4. *Two-dimensional eddy viscosity*

Leith (1969) proposed a two-dimensional eddy viscosity which could be used in atmospheric turbulence models. Although this diffusion scheme has been used only sparsely by meteorological researchers in the past, we thought it might be an attractive scheme to attempt to incorporate into

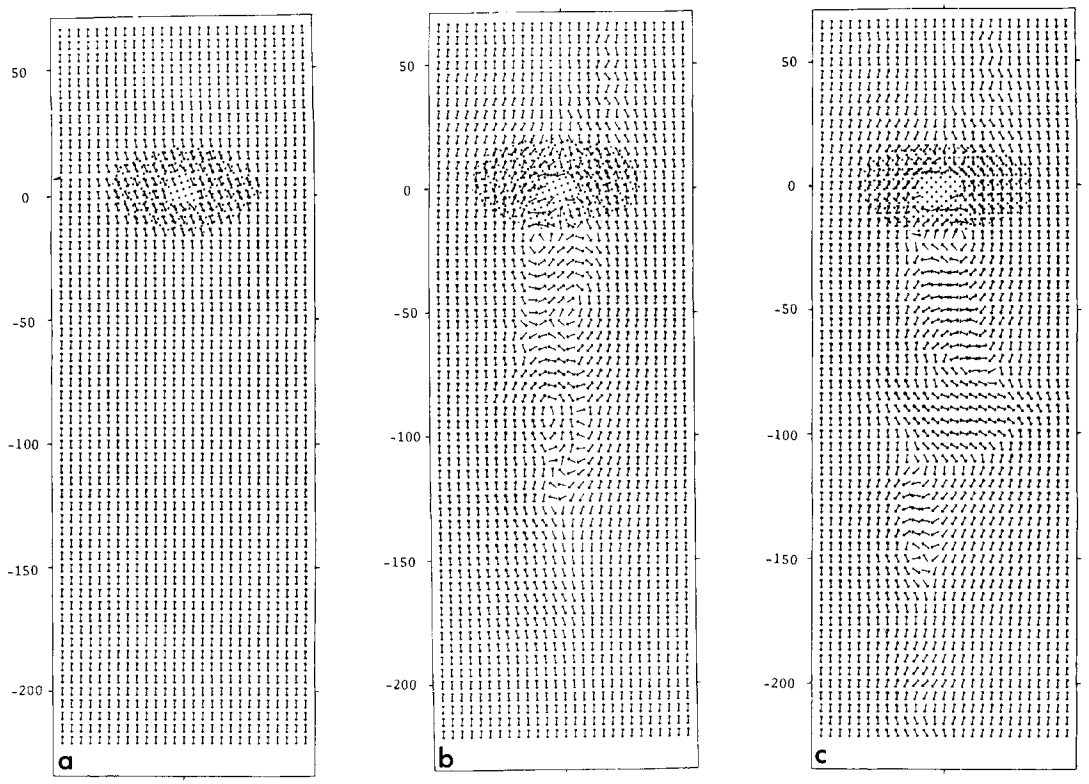

Fig. 5. As in Fig. 4 but for Exp. C; $\Delta s = 5$ km. (a) initially, (b) $t = 5.83$ hours, (c) $t = 8.76$ hours.

our model, whose mean flow is essentially horizontal.

The equation for this eddy viscosity is given in (4). Although Crowley (1969) implied a value of 3.7 for γ_2, we found, using the 5 km grid, that apparently satisfactory results were only obtained using much smaller values of about 0.02. (Another test indicated that 0.04 would have been equally satisfactory.) The results of these runs show virtually no difference when compared to Exp. C's results; see Fig. 6 for an integration time of 5.8 h and $\gamma_2 = 0.02$. With this value of γ_2 the eddy viscosities were about 75% as large within the vortex street as in Exp. C.

For purposes of comparison with laboratory studies, the results shown in Fig. 5b will be used, although we could as well have chosen the results from the experiments using Leith's diffusion scheme.

6. Comparison studies

A numerical simulation of the vortex street of February 17, 1975 has been obtained in Exp. C. Whether or not this result compares favorably with that observed can be decided by analyzing the values of the non-dimensional parameters presented in Section 4. The parameters for the observed case should be roughly matched by the parameters for the simulated case.

The vortex street observed near Cheju-do on February 17, 1975 was studied by Jensen and Agee (1978). They provided an empirical analysis of the observed case which included measurement of the spacing ratio and inferences regarding the Reynolds number, Strouhal number, and effective eddy viscosity. Rather than use their values, however, we will estimate new values which correspond to the particular case observed. These values will be compared to values of the same parameters computed for the simulated vortex street.

By direct measurement from satellite photographs, the spacing between vortices along the same row is found to be $a = 77$ km. The distance between the rows for the vortex pair nearest Cheju-do is $b = 33$ km. The reason for making the measurement closest to the obstacle is to avoid the

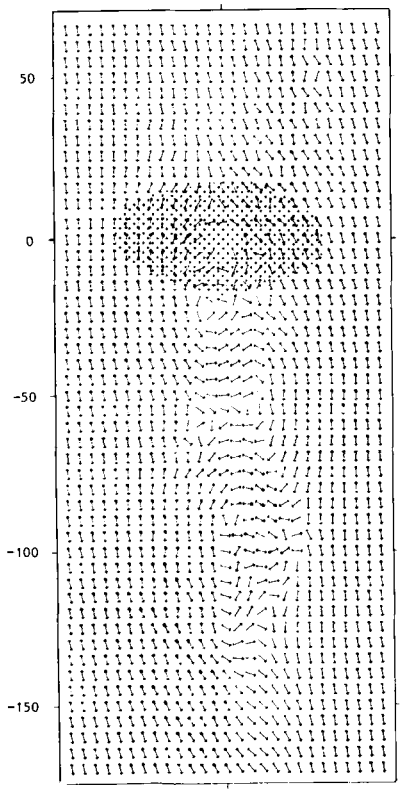

Fig. 6. As in Fig. 5b but for Exp. D.

complication commonly observed that the distance between rows increases downstream. Jensen and Agee (1978) gave the estimate of $b \simeq 50$ km and $b/a \simeq 0.5$, and our direct measurement gives $b/a = 0.43$.

The speed ratio was not discussed by Jensen and Agee; they used a value of 8 m s^{-1} for the mixed-layer wind speed. The mean flow speed outside the wake region at 6 h in Exp. C was 9.9 m s^{-1}. By measuring the travel time and distance for cell #1C, the resulting eddy speed is 7.4 m s^{-1}, which gives a speed ratio of 0.75.

The Reynolds number is perhaps the most uncertain parameter because one might assume that the horizontal eddy diffusivity is representative of a mixed-layer eddy viscosity, which Chopra and Hubert (1965) and Jensen and Agee (1978) suggest should be used in defining the Reynolds number. From observations of the mixed-layer height during the occurrence of the vortex street ($h = 944$ m) and the surface heat flux ($Q_0 = 0.1$ K m s^{-1}, Wyngaard et al., 1978) Jensen and Agee state that the mixed-layer viscosity is $O(w_* h)$, where w_* is the convective velocity scale (Deardorff, 1973) defined by

$$w_* = \left(\frac{g}{T_0} Q_0 h\right)^{1/3}.$$

For $K_y = \frac{1}{2}$ (d/dt) $\overline{y'^2}$, where $\overline{y'^2}$ is the lateral variance of particles diffusing in the mixed layer, from Deardorff and Willis (1975) we find, for rather large diffusion times, that

$$K_y = 0.15 w_* h \simeq 210 \text{ m}^2 \text{ s}^{-1}. \quad (7)$$

However, the average value of the model viscosity (K_y) in the vicinity of the vortex street in Exp. C was 760 m^2 s^{-1}. (In the absence of an island or other feature to generate flow disturbances, the model would predict $K_y = 0$ or molecular value from (3) or (4).) The average width of the obstacle in the mixed layer was 30 km (we use this value rather than the width at the top of the mixed layer because the model presumably senses the obstacle diameter averaged vertically throughout the mixed layer, not just at the top where a vortex street may be visible in the clouds). Using a wind speed of 9.9 m s^{-1}, the Reynolds number is then 390, versus 1400 using (7) or versus Jensen and Agee's estimate of 200.

The Strouhal number may be estimated by measuring a period of shedding for the vortices. The observed case has a period of 2.9 hours, which gives a Strouhal number of 0.18. The simulated case had a period of 2.7 hours, which gives a value of S = 0.19. Lin's parameter is found to be $\beta = 9.0 \times 10^{-4}$ for the observed case and $\beta = 4.9 \times 10^{-4}$ for the simulated case. The spacing ratio for the simulated case is $b/a = 23$ km/70 km = 0.33.

Table 1 summarizes the values for the five important non-dimensional parameters for both the observed and simulated cases. There is good agreement among most of the numbers. Although the appropriate effective Reynolds number to compare against is uncertain, there is evidence (shown in graphical form by Jensen and Agee (1978), taken from work first performed by A. Roshko) that vortex characteristics are not very Re dependent within a certain range of Re. The spacing ratio is a little lower for the model as a result of our smaller b. Related to this underestimate of b by the model is the lack of sufficient lateral spreading of the rows downstream in the simulated results.

The vortices have been accurately resolved in the

Table 1. *Comparison of non-dimensional parameters*

Parameter	Observed case	Simulated case
Speed ratio	0.8*	0.75
Spacing ratio	0.43	0.33
Strouhal number	0.18	0.19
Reynolds number	~200	390
Lin's parameter	9.0×10^{-4}	4.9×10^{-4}

Note: * The value used here is an average value for atmospheric vortex streets.

downstream direction, where we have a ratio of wavelength to grid size of 14:1. However, the cross-stream resolution exhibits a ratio of only 4½:1. This may explain the poorer correspondence between the observed and simulated cases in parameters involving the cross-stream distance, *b*.

In comparing streamlines from the simulation against cloud "streaklines" from the satellite picture, we notice that the simulation exhibits fewer rotational cells—they damp out too quickly with distance. However, the cells far downstream in the satellite picture might be remnants—the clouds may persist after the motions have died away. Because there is no actual wind data to verify the motions associated with the vortices, it is not definitely known which cells are active and which (if any) are remnants.

7. Summary and conclusions

A two-dimensional model of the atmospheric PBL has been presented as an alternative to a 3D model for studying horizontal motions with strong vertical mixing. The surface layer, inversion layer, and overlying stable layer must all be parameterized in such a mixed-layer model. The primary goal of this study was the numerical calculation of the atmospheric analog of the Kármán vortex street under these conditions.

In the experiments involving a mountain island deeply submerged within the mixed layer, a very weak sinusoidal waviness is found, but no vortex street. For a mixed layer which is barely deep enough to allow no part of the mountain to protrude, there was a more pronounced waviness but still no vortices. This result may not hold, however, for boundary layers with poor vertical mixing. Increased atmospheric stability may enhance the barrier effectiveness as a vortex street producer (Trischka, 1980).

Experiment C yielded positive results in comparison. The speed ratio, spacing ratio, and Strouhal number agreed rather closely with observations. Uncertainty in the evaluation of the eddy coefficient and in an effective width of the obstacle produce significant uncertainty in the appropriate values of the eddy Reynolds number and Lin's parameter.

In future studies, further reduction in the grid spacing would appear desirable to allow even better resolution of the vortices. An attempt should also be made at simulating the mixed-layer clouds themselves, perhaps shedding some light on the actual behaviour of the vortex street within the clouds.

8. Acknowledgements

The authors would like to thank Dr Young-June Han for his valuable comments and suggestions during the course of this study and William McKie and Robert Mobley for providing graphics support. This work was sponsored by the National Science Foundation under grant ATM 7724559 and by the National Aeronautics and Space Administration through grant NAG 5-51. Partial support for computations on a CYBER 170/720 was generously provided by the Oregon State University Computer Center.

REFERENCES

Abernathy, F. H. and Kronauer, R. E. 1962. The formation of vortex streets. *J. Fluid. Mech. 13*, 1–20.

Agee, E. M. and Lomax, F. E. 1978. Structure of the mixed layer and inversion layer associated with patterns of mesoscale cellular convection during AMTEX 75. *J. Atmos. Sci. 35*, 2281–2301.

Anthes, R. A., Keyser, D. and Deardorff, J. W. 1982. Further considerations on modeling the sea breeze with a mixed-layer model. To appear in *Mon. Wea. Rev. 110*.

Anthes, R. A., Seaman, N. L. and Warner, T. T. 1980. Comparisons of numerical simulations of the planetary boundary layer by a mixed-layer model and multi-level model. *Mon. Wea. Rev. 108*, 365–376.

Arakawa, A. and Lamb, V. R. 1977. Computational design of the basic dynamical process of the UCLA general circulation model. In *Methods of Computational Physics, Volume 17*: General circulation models of the atmosphere (ed. J. Chang,). New York: Academic Press, 174–265.

Batchelor, G. K. 1967. *An Introduction to Fluid Dynamics*. London: Cambridge University Press, 615 pp.

Chen, J. H. 1973. Numerical boundary conditions and computational modes. *J. Comp. Phys. 13*, 522–535.

Chopra, K. P. and Hubert, L. F. 1964. Kármán vortex streets in the Earth's atmosphere. *Nature 203*, 1341–1343.

Chopra, K. P. 1965. Mesoscale eddies in wake of islands. *J. Atmos. Sci. 22*, 652–657.

Crowley, W. P. 1969. A global numerical ocean model: part I. *J. Comp. Phys. 3*, 111–147.

Deardorff, J. W. 1973. Three-dimensional numerical modeling of the planetary boundary layer. In *Workshop on Micrometeorology* (ed. D. A. Haugen). Boston: American Meteorological Society, 271–311.

Deardorff, J. W. and Willis, G. E. 1975. A parameterization of diffusion into the mixed layer. *J. Appl. Meteorol. 14*, 1451–1458.

Fromm, J. and Harlow, H. 1963. Numerical solution of the problem of vortex street development. *Phys. Fluids 6*, 975–981.

Gaster, M. 1969. Vortex shedding from slender cones at low Reynolds numbers. *J. Fluid Mech. 38*, 565–576.

Gaster, M. 1971. Vortex shedding from circular cylinders at low Reynolds numbers. *J. Fluid Mech. 46*, 749–756.

Gerrard, J. H. 1966. The mechanics of the formation region of vortices behind bluff bodies. *J. Fluid Mech. 25*, 401–413.

Haltiner, G. J. 1971. *Numerical Weather Prediction*. New York: John Wiley & Sons, Inc., 317 pp.

Hirota, I. and Miyakoda, K. 1965. Numerical simulation of Kármán vortex street behind a circular cylinder. *J. Meteorol. Soc. Japan, Ser. II 43*, 30–41.

Jensen, N. O. and Agee, E. M 1978. Vortex cloud street during AMTEX 75. *Tellus 30*, 517–523.

Kármán, Th. von 1911. Über den mechanisms des widerstandes den ein bewegter körber in einer flüssigkeit erfährt. *Gottingen Nachrichten Math.-Phys.* 509–517.

Keyser, D. and Anthes, R. A. 1977. The applicability of a mixed-layer model of the planetary boundary layer to real-data forecasting. *Mon. Wea. Rev. 105*, 1351–1371.

Klemp, J. B. and Lilly, D. K. 1978. Numerical simulation of hydrostatic mountain waves. *J. Atmos. Sci. 35*, 78–107.

Klemp, J. B. and Wilhelmson, R. B. 1978. The simulation of three-dimensional convective storm dynamics. *J. Atmos. Sci. 35*, 1070–1096.

Kovásznay, L. S. G. 1949. Hot-wire investigation of the wake behind circular cylinders at low Reynolds numbers. *Proc. Roy. Soc. (London), Ser. A 198*, 174–190.

Lamb, H. 1932. *Hydrodynamics*, 6th ed. London: Cambridge University Press, 738 pp.

Lavoie, R. L. 1972. A mesoscale model of lake-effect storms. *J. Atmos. Sci. 29*, 1025–1040.

Lavoie, R. L. 1974. A numerical model of trade wind weather on Oahu. *Mon. Wea. Rev. 102*, 630–637.

Leith, C. C. 1969. Two dimensional eddy viscosity coefficients. In *Proceedings of the WMO-IUGG Symposium on Numerical Weather Prediction*, Tokyo, Nov. 1968, Sec. I, 41–44.

Lilly, D. K. 1968. Models of cloud-topped mixed layers under a strong inversion. *Quart. J. Roy. Meteorol. Soc. 94*, 292–309.

Lyons, W. A. and Fujita, T. 1968. Mesoscale motions in oceanic stratus as revealed by satellite data. *Mon. Wea. Rev. 96*, 304–314.

Matsuno, T. 1966. Numerical integrations of the primitive equations by a simulated backward difference method. *J. Meteorol. Soc. Japan, Ser. II 44*, 76–84.

Mesinger, F. and Arakawa, A. 1976. Numerical methods used in atmospheric models, Vol. I. *GARP Publication Series*, No. 17. Geneva: World Meteorological Organization/ICSU, 64 pp.

Miyakoda, K. and Rosati, A. 1977. One-way nested grid models: the interface condition and numerical accuracy. *Mon. Wea. Rev. 105*, 1092–1107.

Nitta, T. 1964. On the reflective computational wave caused by the outflow boundary condition. *J. Meteorol. Soc. Japan, Ser. II 42*, 274–276.

Orlanski, I. 1976. A simple boundary condition for unbounded hyperbolic flows. *J. Comp. Phys. 21*, 251–269.

Overland, J. E., Hitchman, M. H. and Han, Y.-J. 1979. A regional surface wind model for mountainous coastal areas. *NOAA Tech. Rept.*, ERL 407–PMEL 32, U.S. Department of Commerce. (Available from Superintendent of Documents, USGPO, Washington, DC 20402, USA. Order by SD Stock No. 003-017-00461-9.)

Pao, H. P. and Kao, T. W. 1976. On vortex trails over ocean islands. *Atmos. Sci.* (The Meteorological Society of the Republic of China) *3*, 28–38.

Papailou, D. D. and Lykoudis, P. S. 1974. Turbulent vortex streets and the entrainment mechanism of the turbulent wake. *J. Fluid Mech. 62*, 11–31.

Price, J. F., Mooers, C. N. K. and Van Leer, J. C. 1978. Observation and simulation of storm-induced mixed-layer deepening. *J. Phys. Oceanog. 8*, 582–599.

Sadourny, R. 1975. The dynamics of finite-difference models of the shallow water equations. *J. Atmos. Sci. 32*, 680–689.

Smagorinsky, J. 1963. General circulation experiments with the primitive equations: I. The basic experiment. *Mon. Wea. Rev. 91*, 99–164.

Sundström, A. and Elvius, T. 1979. Computational problems related to limited-area modeling. In

"Numerical Methods Used in Atmospheric Models, Volume 2," (Joint Organizing Committee, ed.). *GARP Publication Series*, No. 17. Geneva: World Meteorological Organization/ICSU, 379–416.

Thomson, R. E., Gower, J. F. R. and Bowker, N. W. 1977. Vortex street formation in the wake of the Aleutian Islands. *Mon. Wea. Rev. 105*, 873–884.

Trischka, J. W. 1980. Cone models of mountain peaks associated with atmospheric vortex streets. *Tellus 32*, 365–375.

Tsuchiya, K. 1969. The clouds with the shape of Kármán vortex street in the wake of Cheju Island, Korea. *J. Meteorol. Soc. Japan, Ser. II 47*, 457–464.

Wyngaard, J. C., Pennell, W. T. Lenschow, D. H. and LeMone, M. A. 1978. The temperature-humidity covariance budget in the convective boundary layer. *J. Atmos. Sci. 35*, 47–58.

Zimmerman, L. I. 1969. Atmospheric wake phenomena near the Canary Islands. *J. Appl. Meteorol. 8*, 896–907.